European Journal of Pharmaceutics and Biopharmaceutics 76 (2010) 498–506

Contents lists available at ScienceDirect

European Journal of Pharmaceutics and Biopharmaceutics

journal homepage: www.elsevier.com/locate/ejpb

Research paper

Elucidation of the internal physical and chemical microstructure of pharmaceutical granules using X-ray micro-computed tomography, Raman microscopy and infrared spectroscopy

Barry Crean [a,b,c], Andrew Parker [d,*], Delphine Le Roux [d], Mark Perkins [d], Shen Y. Luk [d], Simon R. Banks [c], Colin D. Melia [b], Clive J. Roberts [a,d]

[a] Laboratory of Biophysics and Surface Analysis, School of Pharmacy, University of Nottingham, Nottingham, UK
[b] Formulation Insights, School of Pharmacy, University of Nottingham, Nottingham, UK
[c] AstraZeneca Charnwood Pharmaceutical Development, Loughborough, UK
[d] Molecular Profiles Ltd., Nottingham Business Park, Nottingham, UK

ARTICLE INFO

Article history:
Received 3 May 2010
Accepted in revised form 22 August 2010
Available online 27 August 2010

Keywords:
High-shear aqueous granulation
α-Lactose monohydrate
Polyvinyl pyrrolidone
X-ray micro-computed tomography
Confocal Raman microscopy

ABSTRACT

X-ray micro-computed tomography (XMCT) was used in conjunction with confocal Raman mapping to measure the intra-granular pore size, binder volumes and to provide spatial and chemical maps of internal granular components in α-lactose monohydrate granules formulated with different molecular weights of polyvinyl pyrrolidone (PVP). Infrared spectroscopy was used to understand the molecular association of binder domains. Granules were prepared by high-shear aqueous granulation from α-lactose monohydrate and PVP K29/32 or K90. XMCT was used to visualise the granule microstructure, intra-granular binder distribution and measure intra-granular porosity, which was subsequently related to intrusion porosimetry measurements. Confocal Raman microscopy and infrared microscopy were employed to investigate the distribution of components within the granule and explore the nature of binder substrate interactions. XMCT data sets of internal granule microstructure provided values of residual porosity in the lactose:PVP K29/32 and lactose:PVP K90 granules of 32.41 ± 4.60% and 22.40 ± 0.03%, respectively. The binder volumes of the lactose:PVP K29/32 and lactose:PVP K90 granules were 2.98 ± 0.10% and 3.38 ± 0.07%, respectively, and were attributed to PVP-rich binder domains within the granule. Confocal Raman microscopy revealed anisotropic domains of PVP between 2 μm and 20 μm in size surrounded by larger particles of lactose, in both granule types. Raman data showed that PVP domains contained various amounts of lactose, whilst IR microscopy determined that the PVP was molecularly associated with lactose, rather than residual water. The work shows that XMCT can be applied to investigate granular microstructure and resolve the porosity and the excipient and binder volumes. Combining this technique with vibrational techniques provides further structural information and aids the interpretations of the XMCT images. When used complementarily, these techniques highlighted that porosity and binder volume were the most significant microstructural differences between the α-lactose monohydrate granules formulated with the different grades of PVP.

1. Introduction

Wet granulation is a size enlargement process in which a liquid binder enables sufficient adhesion between individual powder particles for nucleation and subsequent growth of agglomerates to form granules. A detailed knowledge of granule microstructure is crucial for developing a better understanding of granule behaviour during these stages. Poor granulation can prevent critical quality attributes being achieved e.g., appearance (capping, picking and cracking during the compression) and uniformity of dosage unit (owing to poor granule flow).

There is an increased need for a mechanistic understanding of processes as driven by the International tripartite Conference on Harmonisation (ICH) guidance on Pharmaceutical Development, Quality Risk Management and Pharmaceutical Quality Systems [1–3]. As a consequence of this 'Quality by Design' (QbD) approach, there is a greater need to identify the relationships between critical quality attributes and critical process parameters for any given drug product. To this end, a multifaceted approach to elucidate the physical and chemical structure of granules produced by high-shear aqueous granulation is discussed in this paper.

A deeper understanding of granule microstructure would be beneficial to the QbD approach by identifying granule attributes

* Corresponding author. Molecular Profiles Ltd., 8 Orchard Place, Nottingham Business Park, Nottingham NG8 6PX, UK. Tel.: +44 0 115 871 8888; fax: +44 0 115 871 8889.
E-mail address: aparker@molprofiles.co.uk (A. Parker).

0939-6411/$ - see front matter © 2010 Elsevier B.V. All rights reserved.
doi:10.1016/j.ejpb.2010.08.006

which may subsequently impact on their performance. Surface energy characterisation has been commonly used as a tool for binder selection [4–8] but results have been only indirectly related to granule mechanical properties, for example through measurements of granule friability as a function of time. There are also difficulties with the use of contact angle measurements. These can arise from the effects of sample preparation, for example the choice of test liquids and the compression of powder samples into discs which may alter the material properties of the powder and powder disc roughness [9]. Inverse gas chromatography measurements can also be criticised because high energy sites are preferentially probed at infinite dilution and there are assumptions in quantifying the polar components of total surface energy [10–12].

Direct visualisation of the interior and exterior of granules would enable the formulator to compare binder performance in building the granule structure. It could provide a direct measurement of intra-granular porosity, in contrast to the estimated values obtained from porosimetry, and which rely on absolute connectivity of all pores. This could provide a correlation between formulation, process factors and drug product performance. This assessment would be further enhanced by correlations between the physical properties and chemical structure of the granules.

This study uses XMCT to investigate the internal structures of model granules. This technique allows non-invasive, 3D imaging of internal structure of small objects at micron resolution [13–16] in contrast to conventional techniques such as scanning electron microscopy, which probe the outer surface, but which are destructive if internal structure is to be examined. XMCT acquires a 3D tomography data set of a sample based on the attenuation of X-rays by different components within the sample [13,15–20]. The degree of attenuation reflects both the relative differences in material density and atomic density between different components of the sample.

It has been well documented that XMCT can provide the capability for imaging internal structure of solid dosage forms [21–25] and granules [20,23,26–29]. Farber et al., for instance, compared XMCT and mercury porosimetry for characterising porosity and pore size distributions in granules and concluded that XMCT was a viable technique for both measuring the true size distribution of pores and providing detailed morphological information such as pore shape, spatial distribution and connectivity [22].

In this paper, XMCT was combined with other techniques to build upon the understanding of the tomography data and to provide further information on the chemical properties of the granules and the interaction between different components. Raman mapping was used to provide complementary chemical information at sub-micron lateral resolution, enabling the identification of the constituent components of inhomogeneously mixed matrices [30,31]. Infrared spectroscopy was used at higher wavenumber resolution to determine whether the physical interactions of the povidone binder arose from residual water from the wet granulation step or whether the physical interactions were due to an interaction with the lactose diluent.

This investigation uses the results of XMCT, Raman microscopy and infrared spectroscopy collectively to elucidate the microstructure and chemical properties of pharmaceutical granules, with a view to obtaining a greater understanding of the role of the binder and how two commonly used molecular weights of povidone (PVP) influence the granule attributes.

2. Materials and methods

2.1. Materials

α-Lactose monohydrate, Pharmatose® 450M, was a provided as a gift from DMV International (Holland). PVP, Povidone® K29/32 and K90, were supplied by ISP (Germany). The average molecular mass values of the two PVP grades were 40,000 and 1000,000, respectively, with the K90 grade being of greater viscosity.

2.2. True density measurements

The true densities of the α-lactose monohydrate and both PVP grades were determined using an AccuPyc 1330 Gas (He) Pycnometer (Micromeritics Instrument Corporation, GA, USA). Results are averages of five replicate determinations on the powdered materials as supplied.

2.3. Preparation of granules by high-shear aqueous granulation

Granules were prepared in 50 g batches using a Kenwood CH180 mixer (Kenwood Ltd., UK). Excipients were first sieved through a 500 μm mesh (Endecotts Ltd., UK). The weighed excipients were placed into the granulator bowl and blended dry for 2 min at speed 1 (tip speed $\approx 16.4\ m\ s^{-1} \approx 3400$ rpm measured by laser tachometry (RS Components Ltd., UK)). Water was added at $1\ ml\ min^{-1}$ using a syringe with a needle 0.8 mm in bore diameter. Identical binder levels (3% w/w), water addition levels (14% w/w) and kneading times (6 min) were used for both formulations. The wet granules were passed through a 1.4 mm sieve and tray-dried at 50 °C for 16 h in an oven (Gallenkamp Plus II Oven, Weiss–Gallenkamp, UK) to a final moisture content of 3% w/w. The dried granules were then passed through a 1.0 mm sieve and representative samples taken using a spinning riffler splitter (Microscal Ltd., UK). Granule samples were stored in double-sealed, clean, dry amber glass bottles at room temperature.

2.4. Granule size analysis

Granule size distributions were measured using a Mastersizer® 2000 laser diffractometer fitted with a Scirocco® dry powder feeder (Malvern, UK). Samples were fed into the diffractometer at a vibration feed rate of 70% and a dispersive air pressure of 2 bar. Background readings were recorded (for 10 s at 10,000 background snaps) prior to measurement readings taken at 20,000 measurement snaps for 20 s. The average granule size distribution was measured from three replicates of each sample.

2.5. Granule porosity measurement by mercury porosimetry

Granule porosity and pore volume distributions were measured using an AutoPore IV 9500 high-pressure mercury intrusion porosimeter (Micromeritics Instrument Corporation, GA, USA). Granules were dried in a vacuum oven at 50 °C for 24 h, samples of known mass placed in a calibrated glass penetrometer (penetrometer volume: 6.035 ml) and degassed using a vacuum pump. Volume measurements were taken as the sample was subjected to an intrusion pressure ramp of 1.5 and 60,000 psi (10 kPa to 414 MPa) from three replicates of each sample. The limiting pore size for mercury penetration was then calculated using PoreMaster® v1.05 (Micromeritics) software, assuming parallel, cylindrical non-intersecting pores of different radii, a surface tension of $485\ mN\ m^{-1}$ and an advancing contact angle between mercury and the granular material of 130°. Porosity was calculated from sample bulk density and the total volume of intruded mercury. Intra-granular porosity was calculated using the total intruded volume of mercury measured over the high-pressure range (30–60,000 psi), and this corresponded to pore voids less than 4.8 μm in diameter.

2.6. X-ray micro-computed tomography

Individual similarly sized granules were selected for analysis in a high-resolution X-ray micro-tomograph (SkyScan 1172, SkyScan, Belgium) (n = 3 granules). These single granules were placed within a disposable plastic Eppendorf® pipette tip, which was in turn mounted onto the tomograph sample holder. X-ray shadow images were acquired with an optimised X-ray source at 100 kV (124 μA) and using a 0.40° scan step over 180° total sample rotation. Random sample movement was applied to limit ring artefacts in the final images. Corrections were made for imperfections in the detector output using a flat-field correction procedure. The resolution of the charge-coupled device (CCD) camera was 4000 × 2096 pixels, and the pixel size was ~0.8 μm under the operating conditions used.

The X-ray shadow images were reconstructed into the non-invasive cross-sectional images using NRecon® software (SkyScan). This software implements the Feldkamp algorithm to create a series of horizontal cross-sectional views of the sample. A correction was applied to the images to further remove ring artefacts and to remove beam-hardening effects. Image analysis was performed using the CTAn software (SkyScan). The reconstructed images were processed, using thresholding to a 256-point linear greyscale, to isolate the solid matrix components from each other and from the pores (image binarisation). The appropriate threshold index to distinguish pores and solid components was determined by comparing the reconstructed greyscale image at the highest magnification and the binarised image. Sample volume, porosity and binder distribution were all calculated from the binary images, whilst the morphology of granules was assessed using the true image files. The sizes of the pore and binder domains were measured using a structure thickness distribution. The procedure fits and quantifies the maximum sphere diameter that can be satisfactorily fitted within the irregular shaped object identified in the binarised image analysis of the tomography data. A second, smaller sphere is then fitted to the remaining volume of that pore, and this is repeated down to the resolution limit of the binarised data.

2.7. Confocal Raman microscopy

Cross-sectional surfaces of comparably sized granules were prepared using a diamond knife on an ultra-microtome (PowerTome XL CR-X, RMC Products, Broeckeler Instruments Inc., AZ, USA). Raman spectra were recorded with a CRM200 confocal Raman microscope (WITec, Ulm, Germany), equipped with a 532-nm Nd:YAG laser. The laser excitation beam was focused using a 100× objective (Nikon, UK), and the scattered light was collected using a 180° backscatter regime, with the laser line intensity being suppressed using an edge filter. The Stokes shifted Raman scattering was dispersed using a 600 groove mm^{-1} grating onto a Peltier cooled, Andor CCD (Andor, UK) to capture the spectra. Under these conditions, the spectral resolution was 8 cm^{-1} and the lateral resolution was 500 nm.

Chemical maps were constructed using a serial imaging process, which involved the acquisition of spectra at defined points within an array. The Raman maps of the specific components were obtained using basis analysis fitting on the Witec project software (WITec). This is a chemometric approach that uses the Raman spectra recorded from the reference components (Lactose and PVP) as basis spectra. The weighting of each basis spectrum to each pixel within the image is defined by a least squares fitting procedure.

2.8. Infrared analysis

Transmission infrared spectra were acquired from the granule samples mounted on a Centaurus microscope and attached to a 370 FT-IR Thermo Nicolet spectrometer. Spectra were acquired with a resolution of 4 cm^{-1} and accumulated over 128 scans.

3. Results and discussion

3.1. Microstructure and physical properties using XMCT and mercury porosimetry

Granule size distributions determined by laser diffraction, for the lactose:PVP K29/32 and lactose:PVP K90 granules, are shown in Fig. 1A. Lactose:PVP K29/32 granules exhibited a bimodal size distribution, whereas lactose:PVP K90 granules exhibited a broad monomodal distribution, whose modal average diameter was similar to the diameter determined for the larger second peak of the lactose:PVP K29/32 granules. The structural integrity of the granules is an important attribute during wet granulation, as granule growth and granule breakage processes occur simultaneously [32] and are influenced by both experimental parameters and material properties. During granulation, granules require a critical dynamic strength to withstand shear and continue to grow [33] and further experimental evidence would be required, beyond the scope of this investigation, to understand the root causes for the differences in size distributions observed.

Intra-granular residual porosities were determined by mercury porosimetry and were found to be 7.0 ± 0.8% and 4.2 ± 0.6% (n = 3)

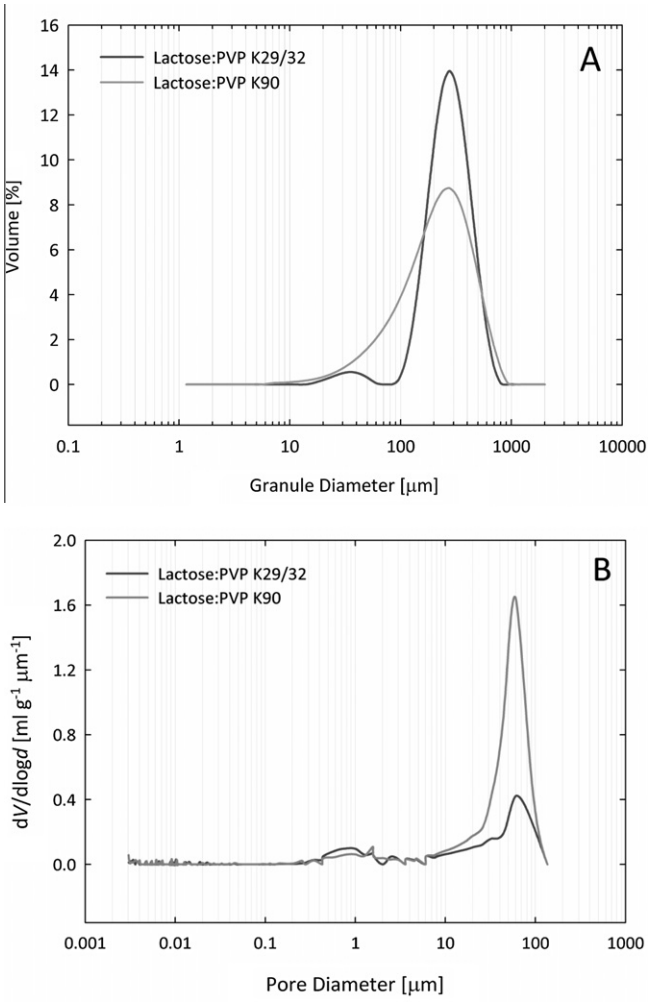

Fig. 1. (A) Size distributions of lactose:PVP granules measured by laser diffractometry. (B) Pore size distributions of lactose:PVP granules measured by mercury porosimetry.

for the lactose:PVP K29/32 and lactose:PVP K90 granules, respectively. Pore size distributions are shown in Fig. 1B. It is interesting to note that whilst the residual porosity of the lactose:PVP K29/32 granules is 67% greater than the lactose:PVP K90 granules, the pore size and pore size distributions are smaller compared with lactose:PVP K90 granules. Consequently, the pore number density in the lactose:PVP K29/32 granules are almost an order of magnitude higher than the lactose:PVP K90 granules, as qualitatively evident when comparing Fig. 1A and B.

Typical reconstructed XMCT images illustrating the internal microstructure of the lactose:PVP K29/32 and lactose:PVP K90 granules are illustrated in Fig. 2A and B, respectively. These images are representative, 2D non-invasive cross-sections reconstructed from the complete image data set (~500 sections). The data are presented on a relative greyscale, such that the least dense regions within the image are black (e.g., air regions) and the densest regions are white. XMCT analysis revealed comparable gross morphologies for both granule types, with each showing an open porous structure.

Each granule type was shown to consist of a grey matrix, which contained a number of relatively dense (white) particles. In order to better visualise the distribution of the denser domains, a representative binarised image where the dense white particles have been isolated in the matrix, for the lactose:PVP K29/32 and the lactose:PVP K90 granules, is presented in Fig. 2C and D, respectively. Qualitatively, the binarised images suggest that the dense domains are better distributed and more finely dispersed in the lactose:PVP K29/32 granule than the lactose:PVP K90 granule, suggesting more efficient mixing for the former under the same granulation conditions. These dense domains have been assigned to the PVP binder (chemically confirmed by the confocal Raman mapping data presented below). This assignment in the tomography data is counter-intuitive when considering the true densities of the crystalline diluent (lactose) and amorphous binder (PVP) determined from helium pycnometry, which were α-lactose monohydrate 1.5453 ± 0.0007 g cm^{-3}, PVP K29/32 1.1962 ± 0.0005 g cm^{-3} and PVP K90 1.2099 ± 0.0003 g cm^{-3} (mean ± SD; $n = 5$), as X-ray attenuation has, in part, a proportional relationship to material density. However, the significant difference in elemental content of PVP compared to lactose (i.e., presence of nitrogen) also will strongly effect the relative X-ray attenuations of each excipient and, in this study, it would appear that the averaged relative molecular mass of elements present is a more influencing factor than the relative material densities for X-ray attenuation of each excipient.

Numerous pores and voids (black domains) can be identified within both binarised images. Qualitative observation suggests that these pores appear to be more prevalent in the lactose:PVP K29/32 granules than the lactose:PVP K90 granules, agreeing with the interpretations of the laser diffraction and mercury porosimetry data and inferred pore number density.

Measurements of binder and pore volumes calculated from binarised data sets are shown in Table 1. The lactose volume is also indicated and is assumed to be the net volume not accounted for by the pores and the binder.

The number of binder domains identified with a size greater than the resolution of the images was greater in the lactose:PVP

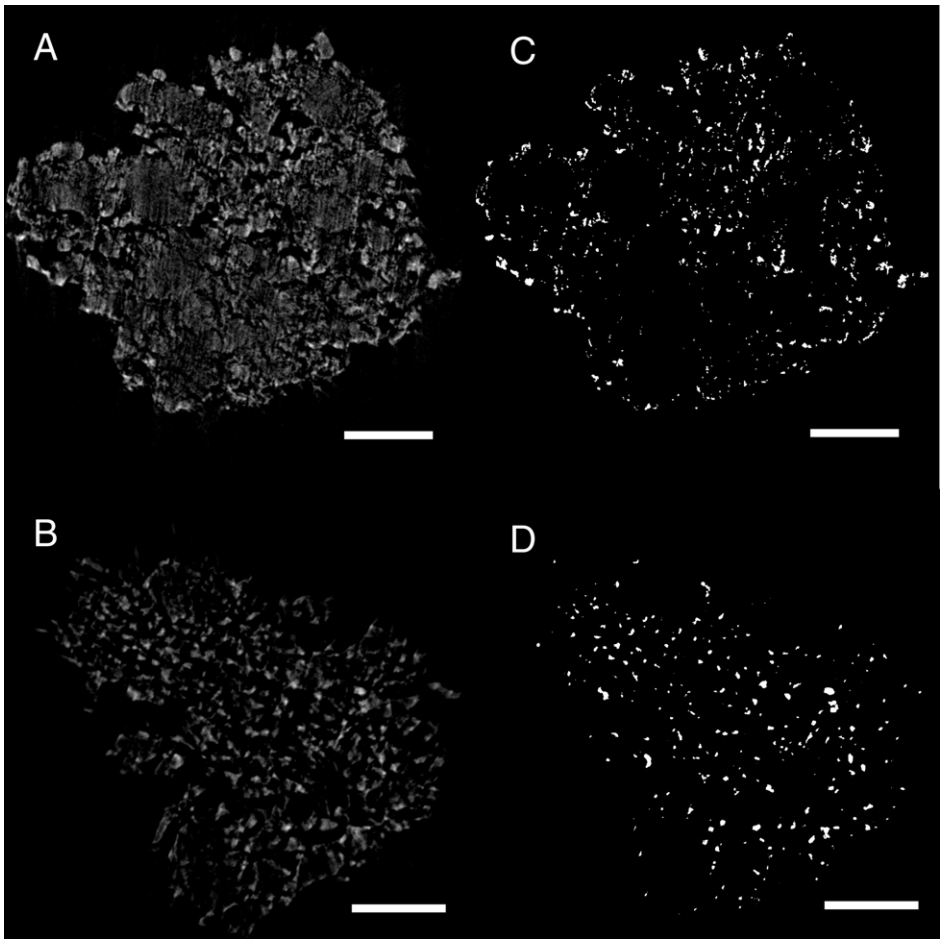

Fig. 2. Representative XMCT images of lactose:PVP granules. Cross-sectional images are shown in the left-hand column ((A) lactose:PVP K29/32 and (B) lactose:PVP K90) and intra-granular binder distributions calculated from binarised images in the right-hand column ((C) lactose:PVP K29/32 and (D) lactose:PVP K90) (scale bars = 200 μm).

Table 1
A comparison of granule microstructure from volume analysis, as measured by XMCT (mean ± SD; $n = 3$ individual granules for each formulation).

Granule	% Total volume		
	Lactose	Binder	Pores
Lactose:PVP K29/32	64.61 ± 2.15	2.98 ± 0.10	32.41 ± 4.60
Lactose:PVP K90	74.22 ± 0.08	3.38 ± 0.07	22.40 ± 1.03

K90 than in the K29/32 granules. This provides further evidence that under the same granulation conditions, lactose:PVP K90 did not disperse through the moist powder blend as effectively as PVP K29/32. This may be a consequence of the higher viscosity of the K90 grade polymer.

The data also revealed that the lactose:PVP K29/32 granule was more porous (by 45%) than the lactose:PVP K90 granule when measured by XMCT. This is in good agreement with the mercury porosimetry data.

The porosity measurements from mercury porosimetry and XMCT demonstrated that the lactose:PVP K29/32 granules were more porous than the lactose:PVP K90 granules by a factor of approximately 1.5. However, the absolute values for porosity determined from XMCT (32.4% v/v and 22.4% v/v, respectively) were considerably higher than those from porosimetry (7.0% v/v and 4.2% v/v, respectively), and this variability probably arises from the intrinsic difference in how the two techniques measure porosity. Whilst mercury porosimetry permits the measurement of a population of smaller pores than XMCT (it can measure pores upwards of 3 nm in diameter [34]), it cannot differentiate between intra- and inter-granular porosity [35] and cannot access closed pores. In contrast, XMCT can access both open and closed pore populations and is a direct measurement which is limited only by the resolution of the images. Previously, Farber et al. have reported that XMCT can be less precise in measuring total porosity than mercury porosimetry, although it can provide detailed information on intra-granular pore-geometry and distribution owing to the finite spatial resolution [22]. It is significant that the tomography used for the work reported in this paper has a better spatial resolution (ca. 1 μm) than the equipment used in the study by Farber et al. (4 μm). Hence, measurements of intra-granular porosity presented here should provide a more accurate estimation of porosity. It is likely that the increase in porosity in the granules relates to the closed pores not accessible by mercury porosimetry.

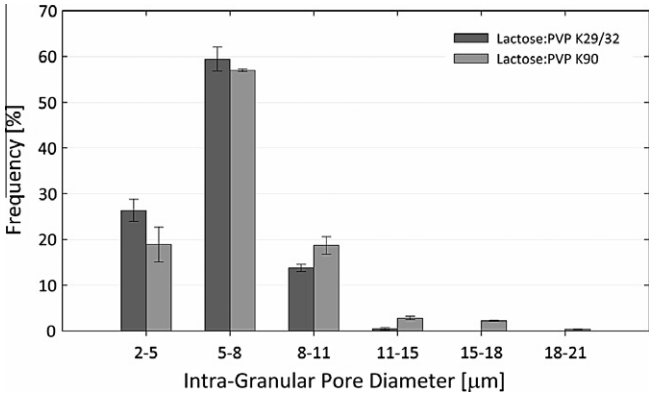

Fig. 3. Intra-granular pore size distributions of lactose:PVP granules as measured by XMCT (mean ± SD; $n = 3$ individual granules for each formulation).

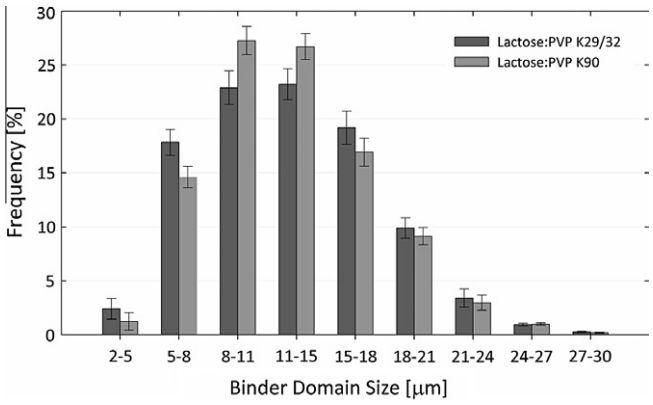

Fig. 4. Size distribution of intra-granular binder domains (mean ± SD; $n = 3$ individual granules for each formulation).

The size distributions of the pores and the binder domains from the XMCT data are illustrated in Figs. 3 and 4, respectively. The trend in the pore size distributions indicate that pores in the granules containing lactose:PVP K90 are typically larger when compared with the lactose:PVP K29/32 containing granules (agreeing with the mercury porosimetry data). The population of binder domains in each granule type was similar in each binned grouping across the size range detected, with no differential trend between granule type observable.

However, an important point was that the total number of binder domains detected was greater for the lactose:PVP K90 granule by ca. 13% which, as commented previously, is most likely due to the less efficient spreading of the higher molecular weight K90 grade PVP. Over 60% of the particles identified for each granule type were present in the 2–15 μm size range.

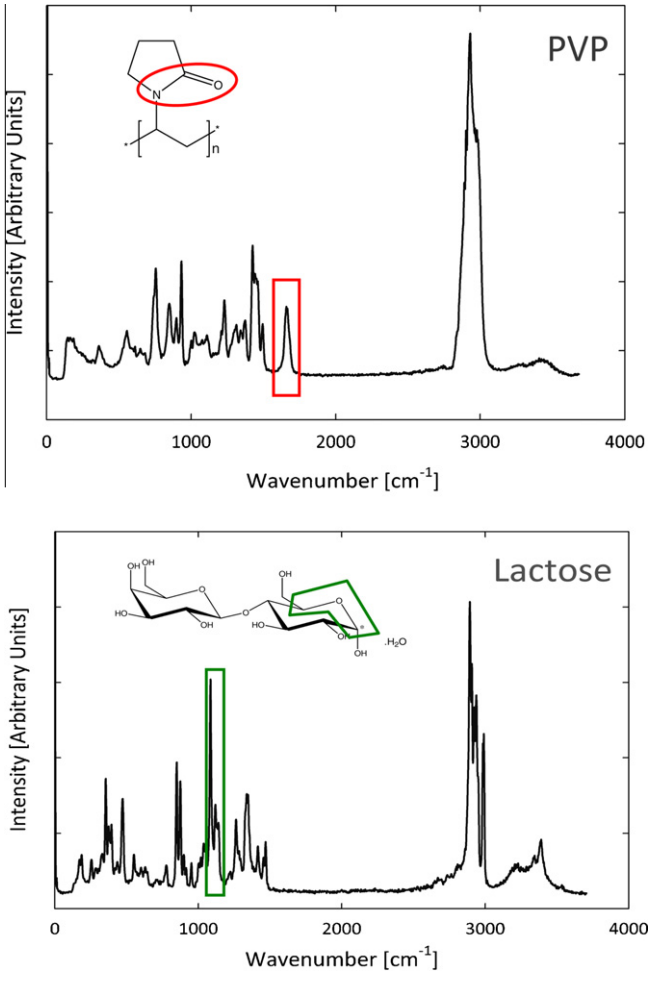

Fig. 5. Raman fingerprint spectra for lactose and PVP. The endocyclic glucopyronosyl ether bond (1118 cm^{-1}) and the COH bonds (1080 cm^{-1}) were used to confer specificity for lactose, and the amide bond (1679 cm^{-1}) was representative of PVP.

3.2. Determination of microstructure and chemical properties by confocal Raman microscopy and infrared spectroscopy

Whilst XMCT successfully delineated regions consistent with being PVP-rich (likely to be unprocessed PVP from the wet granulation step) from the other matrix material, it was unable to resolve the degree of homogeneity of PVP coating the lactose regions in the matrix.

In order to further understand the distribution of components within the granule structure, confocal Raman mapping was performed on cross-sectioned granule surfaces. Spectra of the pure α-lactose monohydrate and the PVP powders were obtained for reference (Fig. 5) and were compared to literature spectra [36,37] to ensure they were specific for the intended components and free from contamination.

Typical 2D Raman chemical maps from the lactose:PVP granules are illustrated in Fig. 6. The chemical structure of both granule

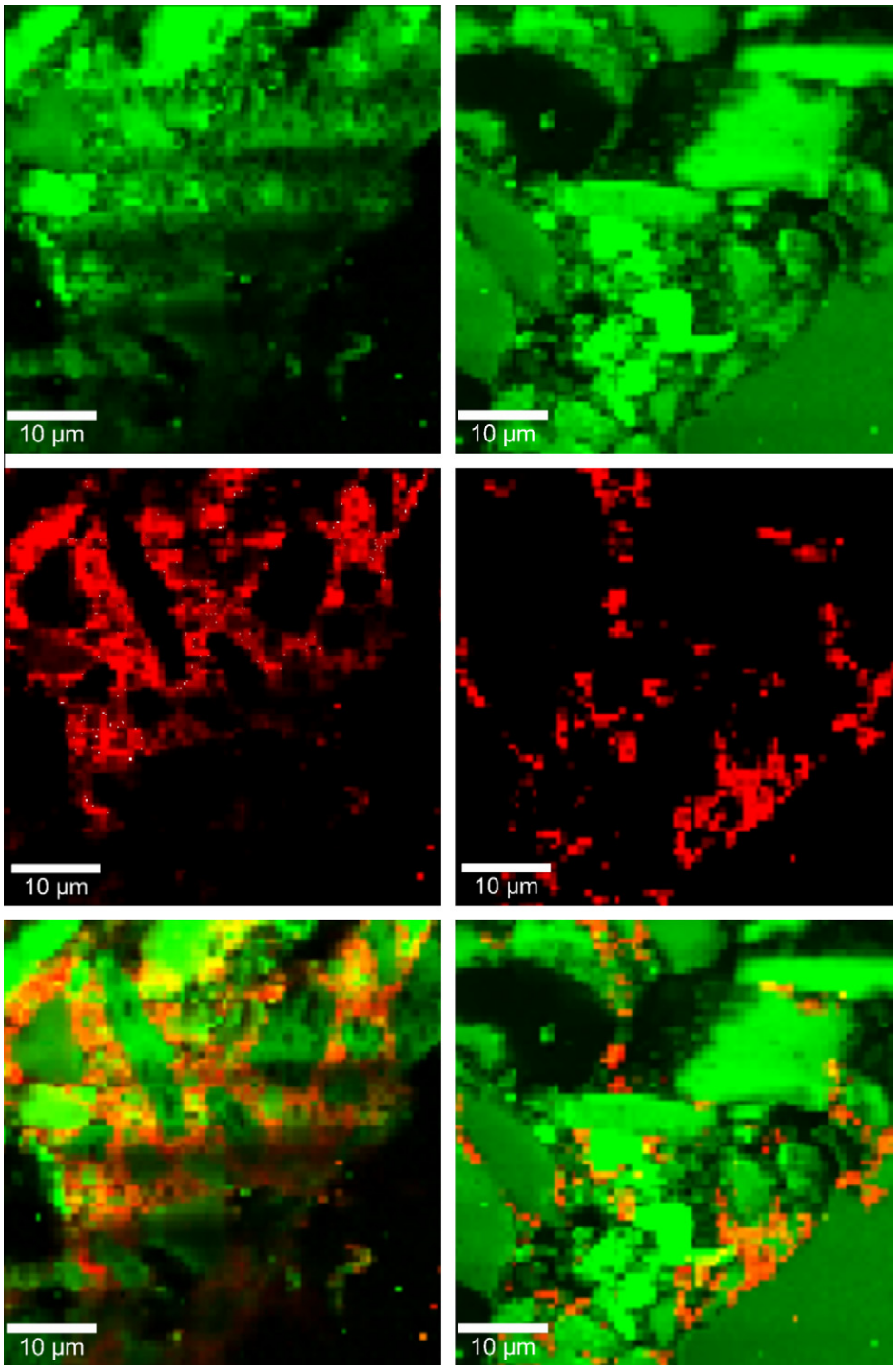

Fig. 6. Raman maps of granule cross-sections. Raman maps of a cross-section of a granule surface are shown where each pixel represents a Raman spectrum. Maps of lactose:PVP K29/32 granules are shown on the left column and lactose:PVP K90 granules are shown in the right-hand column. Green pixels represent α-lactose monohydrate reference spectrum, red pixels represent PVP, yellow/orange pixels where both are present in the overlay and black pixels represent porous regions. (For interpretation of the references to colour in this figure legend, the reader is referred to the web version of this article.)

types display small, anisotropically shaped domains of PVP (ca. 2–20 μm) identified between the larger particles of lactose. These domains correlate with the denser domains identified in the binarisation of the XMCT data and for each granule type (Fig. 2C and D), and the distribution of PVP was spatially comparable at the micron length scale.

A closer inspection of the chemical maps suggests the PVP is not located in discrete domains but located concomitantly with the lactose. To confirm these observations, spectra were extracted from different regions of the images for a lactose:PVP K29/32 granule, and these are compared with the reference spectra, in Fig. 7.

Spectra extracted around point A were shown to consist only of lactose as indicated by the presence of intense peaks at 1080 and 1118 cm^{-1} (CO and COH) and the absence of any peak at 1679 cm^{-1} (amide/PVP).

In contrast, spectra extracted from points B and C display evidence of the amide peak in the region 1660–1680 cm^{-1} indicative of PVP, with the amide peak present at differing intensities normalised to the lactose peak at 1080 cm^{-1}.

From these results, it can be inferred that PVP is present in differing sized domains (or layer thicknesses) over the surface of the α-lactose monohydrate particles exposed in the granule cross-sections. The presence of a lactose-only domain present does not necessarily mean that it was an area uncoated by binder during the granulation process as the sample preparation procedure may have exposed the internal bulk of the crystalline diluent. It is likely that PVP does provide a complete surface coverage of lactose, given the number of domains found at the micron length scale that contain both binder and diluent. This indicates efficient processing but cannot absolutely confirm or refute this conclusion owing to the limits imposed by the resolution of the techniques and preparation method.

Given that the stretching of the non-hydrogen bonded amide in PVP exhibits a Raman shift of 1679 cm^{-1} [38–40], another interesting observation is that the amide band was shifted to a lower frequency in comparison with the reference spectrum. This could indicate some interaction at a molecular level, such as hydrogen bonding potentially between PVP and the lactose or residual water remaining from wet granulation. To further examine the nature of any PVP interactions, transmission infrared experiments were performed, with a higher wavenumber resolution than the corresponding Raman data, to better determine any potential peak shifts.

Spectra were recorded from the lactose and PVP reference powders and from each type of granule. The granules were then heated in the oven at 110 °C for 45 min to remove any residual-free water.

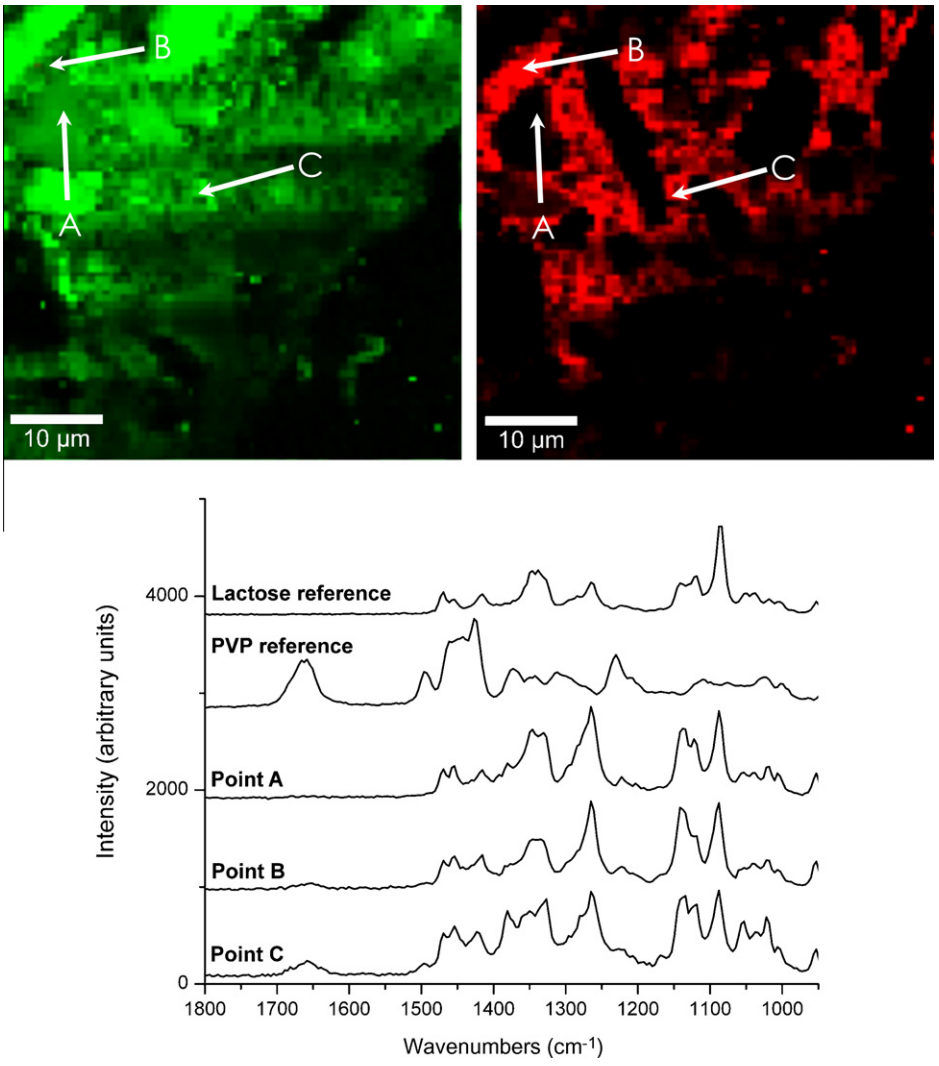

Fig. 7. Raman microscopy of lactose:PVP K29/32 granule cross-section. Raman maps of a surface from a granule cross-section are shown where each pixel represents a Raman spectrum. Point A represents a lactose crystal, point B represents a relatively thin layer of PVP resting on a lactose crystal and point C interrogates a relatively thick layer of PVP resting a lactose crystal. Raman spectra at these points are also shown.

This temperature was chosen so that it would not affect lactose monohydrate, whose dehydration occurs at ~147 °C [41]. The conservation of lactose in the hydrate form is confirmed by the presence of the peak at 3520 cm^{-1} (Fig. 8).

The PVP peak at 1678 cm^{-1} shifts to 1664 cm^{-1} (Fig. 9) when this compound is mixed with lactose monohydrate, and because this shift remains after heating the granule, it cannot be attributed to hydrogen bonding between PVP and water, but is more likely related to hydrogen bonding between lactose and PVP [42]. Similar downward shifts in peak frequency have been noticed in previous studies of sugar:PVP systems [43].

The combination of Raman mapping and infrared spectroscopy shows significant mixing and diluent:binding bonding in both granule types, complementing the information gathered from the XMCT. This interpretation agrees with the high-speed DSC analysis of solid-state properties of lactose:PVP granules in which it was suggested that lactose forms a saturated solution with PVP during wet granulation. The reduction in glass transition temperature indicated the intimate mixing of lactose and PVP and that the amorphous state contained equal proportions of PVP and lactose [44].

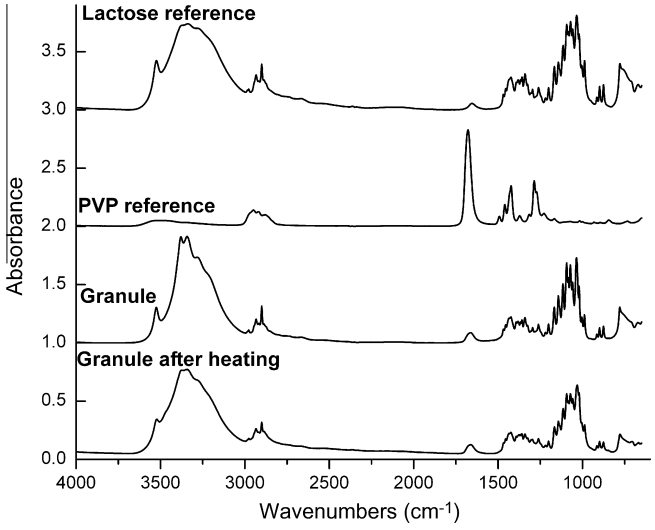

Fig. 8. Transmission infrared spectra between 4000 and 650 cm^{-1} of lactose reference, PVP reference, lactose:PVP K29/32 granule before and after heating to 110 °C for 45 min.

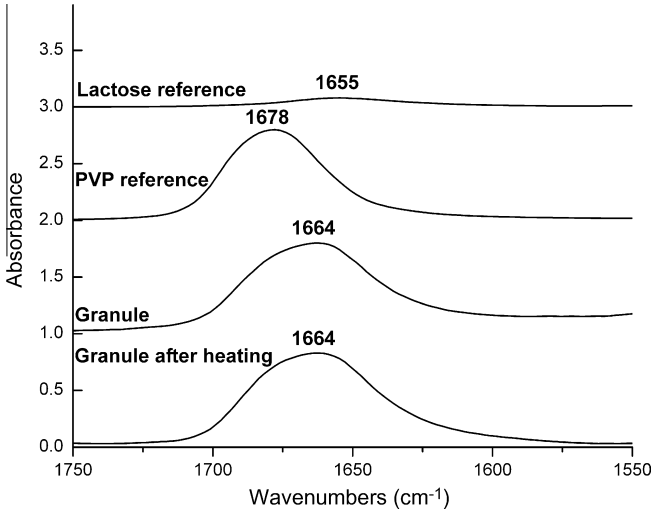

Fig. 9. Transmission infrared spectra between 1750 and 1550 cm^{-1} of lactose reference, PVP reference, lactose:PVP K29/32 granule before and after heating to 110 °C for 45 min.

The combination of physical and chemical analytical methods clearly showed four different structural regions are present within both granule types. The localised analysis at the micron length scale using confocal Raman microscopy indicated structural regions consisting of: (i) PVP-coated lactose with PVP in excess, (ii) PVP-coated lactose in which PVP was depleted and (iii) lactose-only domains. Structures (i) and (ii) can be interpreted in terms of different layer thicknesses of PVP on lactose crystals, and (iii) is probably an artefact of sample sectioning. Binarisation image analysis from the XMCT data showed that at the granular level, there were also (iv) discreet and isolated domains of PVP, which may represent PVP that was incompletely processed during the granulation step. When the performance of the two different viscosity grades of PVP were compared, the main microstructural differences occurred in the residual porosity, pore size and pore size distribution, rather than in the chemical structure of the granule.

4. Conclusions

XMCT, confocal Raman microscopy and infrared spectroscopy have been applied to investigate internal granular microstructure. Intra-granular pore, excipient and binder volumes were resolved for lactose:PVP K29/32 and lactose:PVP K90 granules using XMCT. The experiments performed here demonstrate how these parameters varied as a function of binder viscosity. Combining this technique with Raman microscopy provided further information on intra-granular microstructural regions and enabled chemical interpretations of the XMCT images. The infrared spectroscopy measurements suggest that the PVP was molecular associated with the lactose, not the residual water from wet granulation. This combination of analytical techniques showed four microstructural regions were present in the granules, independent of PVP molecular weight. In the future, this combination of techniques may provide a powerful approach for investigations of process optimisation and root cause analysis in granulation processes.

Acknowledgments

B.C. gratefully acknowledges Dr. Walter Cook, Mr. Richard Bell, Dr. Jonathan C.D. Sutch and Ms. Elaine Harrop at AstraZeneca Pharmaceutical Development Charnwood for their assistance in manufacturing granules and Dr. Matthew Bunker at Molecular Profiles Ltd. for many useful discussions during preparation of this manuscript. We would also like to thank AstraZeneca and the EPSRC for funding this work.

References

[1] US Department of Health and Human Services, Food and Drug Administration (FDA), Center for Drug Evaluation and Research (CDER), Tripartite International Conference of Harmonization (ICH): Guidance for Industry, Q8 Pharmaceutical Development, 2006.
[2] US Department of Health and Human Services, Food and Drug Administration (FDA), Center for Drug Evaluation and Research (CDER), Tripartite International Conference of Harmonization (ICH): Guidance for Industry, Q9 Quality Risk Management, 2005.
[3] US Department of Health and Human Services, Food and Drug Administration (FDA), Center for Drug Evaluation and Research (CDER), Tripartite International Conference of Harmonization (ICH): Guidance for Industry, Q10 Pharmaceutical Quality System, 2008.
[4] L. Zajic, G. Buckton, The use of surface-energy values to predict optimum binder selection for granulations, International Journal of Pharmaceutics 59 (1990) 155–164.
[5] R.C. Rowe, Polar non-polar interactions in the granulation of organic substrates with polymer binding-agents, International Journal of Pharmaceutics 56 (1989) 117–124.
[6] R.C. Rowe, Surface free-energy and polarity effects in the granulation of a model system, International Journal of Pharmaceutics 53 (1989) 75–78.

[7] R.C. Rowe, Binder substrate interactions in granulation – a theoretical approach based on surface free-energy and polarity, International Journal of Pharmaceutics 52 (1989) 149–154.
[8] R.C. Rowe, Correlation between predicted binder spreading coefficients and measured granule and tablet properties in the granulation of paracetamol, International Journal of Pharmaceutics 58 (1990) 209–213.
[9] O. Planinšek, A. Trojak, S. Srčič, The dispersive component of the surface free energy of powders assessed using inverse gas chromatography and contact angle measurements, International Journal of Pharmaceutics 221 (2001) 211–217.
[10] K.U. Goss, Considerations about the adsorption of organic molecules from the gas phase to surfaces: implications for inverse gas chromatography and the prediction of adsorption coefficients, Journal of Colloid and Interface Science 190 (1997) 241–249.
[11] C.J. van Oss, M.K. Chaudhury, R.J. Good, Interfacial Lifshitz-van der Waals and polar interactions in macroscopic systems, Chemical Reviews 88 (1988) 927–941.
[12] C.J. van Oss, R.J. Good, M.K. Chaudhury, Additive and nonadditive surface-tension components and the interpretation of contact angles, Langmuir 4 (1988) 884–891.
[13] C.L. Morgan, Principles of Computed Tomography: Combined Translational–Rotational Scanning Systems, Basic Principles of Computed Tomography, University Park Press, Baltimore, USA, 1983. pp. 19–68.
[14] G.N. Hounsfield, Computerized transverse axial scanning (tomography).1: description of system, British Journal of Radiology 46 (1973) 1016–1022.
[15] A.M. Cormack, Representation of a function by its line integrals, with some radiological applications, Journal of Applied Physics 34 (1963) 2722–2727.
[16] A.M. Cormack, Representation of a function by its line integrals, with some radiological applications II, Journal of Applied Physics 35 (1964) 2908–2913.
[17] L.A. Feldkamp, L.C. Davis, J.W. Kress, Practical cone-beam algorithm, Journal of the Optical Society of America A: Optics Image Science and Vision 1 (1984) 612–619.
[18] B.P. Flannery, H.W. Deckman, W.G. Roberge, K.L. Damico, 3-Dimensional X-ray microtomography, Science 237 (1987) 1439–1444.
[19] S.L. Wellington, H.J. Vinegar, X-ray computerized-tomography, Journal of Petroleum Technology 39 (1987) 885–898.
[20] M.A. Ansari, F. Stepanek, The effect of granule microstructure on dissolution rate, Powder Technology 181 (2008) 104–114.
[21] I.C. Sinka, S.F. Burch, J.H. Tweed, J.C. Cunningham, Measurement of density variations in tablets using X-ray computed tomography, International Journal of Pharmaceutics 271 (2004) 215–224.
[22] L. Farber, G. Tardos, J.N. Michaels, Use of X-ray tomography to study the porosity and morphology of granules, Powder Technology 132 (2003) 57–63.
[23] A.M. Bouwman, M.J. Henstra, D. Westerman, J.T. Chung, Z. Zhang, A. Ingram, J.P.K. Seville, H.W. Frijlink, The effect of the amount of binder liquid on the granulation mechanisms and structure of microcrystalline cellulose granules prepared by high shear granulation, International Journal of Pharmaceutics 290 (2005) 129–136.
[24] B.C. Hancock, M.P. Mullarney, X-ray microtomography of solid dosage forms, Pharmaceutical Technology 29 (2005) 92–100.
[25] Y.S. Wu, H.W. Frijlink, L.J. van Vliet, I. Stokroos, K.V.V. Maarschalk, Location-dependent analysis of porosity and pore direction in tablets, Pharmaceutical Research 22 (2005) 1399–1405.
[26] I. Ohno, S. Hasegawa, S. Yada, A. Kusai, K. Moribe, K. Yamamoto, Importance of evaluating the consolidation of granules manufactured by high shear mixer, International Journal of Pharmaceutics 338 (2007) 79–86.
[27] M.A. Ansari, F. Stepanek, Design of granule structure: computational methods and experimental realization, Aiche Journal 52 (2006) 3762–3774.
[28] F. Stepanek, Computer-aided product design – granule dissolution, Chemical Engineering Research & Design 82 (2004) 1458–1466.
[29] P. Rajniak, C. Mancinelli, R.T. Chern, F. Stepanek, L. Farber, B.T. Hill, Experimental study of wet granulation in fluidized bed: impact of the binder properties on the granule morphology, International Journal of Pharmaceutics 334 (2007) 92–102.
[30] G. Turrell, J. Corset, Raman Microscopy: Developments and Applications, Elsevier, London, 1996.
[31] S. Ward, M. Perkins, J.X. Zhang, C.J. Roberts, C.E. Madden, S.Y. Luk, N. Patel, S.J. Ebbens, Identifying and mapping surface amorphous domains, Pharmaceutical Research 22 (2005) 1195–1202.
[32] S.M. Iveson, J.D. Litster, K. Hapgood, B.J. Ennis, Nucleation, growth and breakage phenomena in agitated wet granulation processes: a review, Powder Technology 117 (2001) 3–39.
[33] A.P. Dhanarajan, R. Bandyopadhyay, An energy based population balance approach to model granule growth and breakage in high shear wet granulation processes, AAPS PharmSciTech 8 (2007). Article 66.
[34] T. Allen, Pore Size Determination by Mercury Porosimetry, Particle Size Measurement: Surface Area and Pore Size Determination, vol. 2, Chapman & Hall, London, 1997.
[35] A.M. Juppo, J. Yliruusi, Effect of amount of granulation liquid on total pore volume and pore-size distribution of lactose, glucose and mannitol granules, European Journal of Pharmaceutics and Biopharmaceutics 40 (1994) 299–309.
[36] A. Szép, G. Marosi, B. Marosfői, P. Anna, I. Mohammed-Ziegler, M. Virágh, Quantitative analysis of mixtures of drug delivery system components by Raman microscopy, Polymers for Advanced Technologies 14 (2003) 784–789.
[37] H. Susi, J.S. Ard, Laser-Raman spectra of lactose, Carbohydrate Research 37 (1974) 351–354.
[38] L.S. Taylor, G. Zografi, Spectroscopic characterization of interactions between PVP and indomethacin in amorphous molecular dispersions, Pharmaceutical Research 14 (1997) 1691–1698.
[39] I.A. Degen, Tables of characteristic group frequencies for the interpretation of infrared and Raman spectra, Acolyte Publications, Harrow, 1997.
[40] G. Socrates, Infrared and Raman Characteristic Group Frequencies: Tables and Charts, John Wiley & Sons, Inc., New York, USA, 2001.
[41] A. Szepes, A. Fiebig, J. Ulrich, P. Szabo-Revesz, Structural study of a-lactose monohydrate subjected to microwave radiation, Journal of Thermal and Analytical Calorimetry 89 (2007) 757–760.
[42] L.S. Taylor, F.W. Langkilde, G. Zografi, Fourier transform Raman spectroscopic study of the interaction of water vapor with amorphous polymers, Journal of Pharmaceutical Sciences 90 (2001) 888–901.
[43] L.S. Taylor, G. Zografi, Sugar–polymer hydrogen bond interactions in lyophilized amorphous mixtures, Journal of Pharmaceutical Sciences 87 (1998) 1615–1621.
[44] G. Buckton, A.A. Adeniyi, M. Saunders, A. Ambarkhane, HyperDSC studies of amorphous polyvinylpyrrolidone in a model wet granulation system, International Journal of Pharmaceutics 312 (2006) 61–65.